Extremely slow cation exchange processes in Li_4SiO_4 probed directly by two-time ^7Li stimulated-echo nuclear magnetic resonance spectroscopy

2006 J. Phys.: Condens. Matter 18 9849

(http://iopscience.iop.org/0953-8984/18/43/007)

INSTITUTE OF PHYSICS PUBLISHING JOURNAL OF PHYSICS: CONDENSED MATTER

J. Phys.: Condens. Matter **18** (2006) 9849–9862 doi:10.1088/0953-8984/18/43/007

Extremely slow cation exchange processes in Li_4SiO_4 probed directly by two-time ^7Li stimulated-echo nuclear magnetic resonance spectroscopy

Martin Wilkening and Paul Heitjans

Institut für Physikalische Chemie und Elektrochemie, Leibniz Universität Hannover, Callinstraße 3-3a, 30167 Hannover, Germany

E-mail: wilkening@pci.uni-hannover.de and heitjans@pci.uni-hannover.de

Received 28 July 2006, in final form 12 September 2006
Published 13 October 2006
Online at stacks.iop.org/JPhysCM/18/9849

Abstract

Lithium self-diffusion in the low-temperature modification of polycrystalline lithium ortho-silicate Li_4SiO_4 is investigated by ^7Li two-time stimulated echo NMR spectroscopy. Extremely slow Li exchange processes were directly monitored between 300 and 433 K by recording spin-alignment echoes as a function of mixing time varying over six decades from 10^{-5} to 10 s. In the investigated temperature range the hopping correlation functions show biexponential behaviour. Whereas the first decay step reflects directly Li jumps between electrically different sites, the second one is simply induced by the decay of alignment order due to quadrupolar relaxation. The echo decay rates τ^{-1} (10^1 s$^{-1} \leqslant \tau^{-1} \leqslant 10^4$ s^{-1}), which can be identified with Li jump rates, show Arrhenius behaviour with an activation energy of 0.53(1) eV. The directly measured jump rates are in good agreement with those obtained recently by one- and two-dimensional ^6Li exchange MAS NMR reported in the literature.

(Some figures in this article are in colour only in the electronic version)

1. Introduction

Diffusion of small cations like Li^+ plays an important role in materials science. In particular, for the systematic development of powerful Li ion batteries with high energy density [1, 2], the exact knowledge of Li transport properties is required. For this purpose, cation dynamics of a large number of Li containing materials have been investigated until now. Among other techniques solid state nuclear magnetic resonance (NMR) is increasingly used to characterize the properties of electrode materials; see, e.g., [3]. Besides these application-oriented investigations, NMR is also used to study fundamental aspects of cation diffusion. NMR studies with this aim have been especially common for Li ions [4–7] because of their often high diffusivity and the ease of observing ^7Li NMR. However, only a few Li investigations have been reported so far [8–11], where microscopic diffusion parameters were measured by NMR directly, i.e., without involving a specific theoretical model.

Classical solid state NMR offers a number of techniques probing microscopic as well as macroscopic properties of Li transport [6]. Whereas macroscopic diffusion parameters, in particular the tracer diffusion coefficient, can be measured by static or pulsed field gradient NMR techniques, the analysis of NMR lineshapes and spin–lattice relaxation rates T_1^{-1} provide, in general, access to the atomic jump rate. Although relaxation NMR can be easily applied to a large variety of materials and is capable of revealing information about Li dynamics over wide ranges of temperature T, see, e.g., [12], the interpretation of relaxation data is often theoretically complex. A relatively direct access to the cation jump rate is given only when the diffusion induced relaxation rate maximum at $T = T_{\max}$ on a plot of $\log T_1^{-1}$ versus $1/T$ can be monitored. If the maximum cannot be reached due to thermal instabilities and/or phase transitions of the material, only the low-temperature flank of the $T_1^{-1}(1/T)$-peak is accessible. Relaxation data on the low-T side are sensitive to short-range, i.e. local or within-site, cation motions with low activation energies rather than to long-range diffusion, which is probed on the high-T side [7]. Furthermore, the slope of the low-T flank of a $T_1^{-1}(1/T)$-peak is influenced by correlation effects due to Coulomb interactions of the moving particles and structural disorder of the material [13–15], so that commonly an activation energy is observed which is less than that obtained by macroscopic techniques. The latter value rather corresponds to the slope of the high-T flank, if accessible [7].

The aim of the present paper is to help to establish new NMR techniques which enable a direct, i.e. model independent, measurement of the elementary jump processes.

Two-dimensional (2D) magic angle spinning (MAS) exchange NMR spectroscopy is one approach which can be used to study directly cation dynamics. To our knowledge only a few 2D NMR exchange experiments have been carried out up to now to detect Li diffusion in detail taking advantage of Li chemical shifts [8–11]. However, 2D NMR is applicable only if the exchange process of the Li nuclei between different sites becomes clearly visible in the NMR spectra. Much less time consuming than 2D experiments and applicable to a much broader class of Li containing crystalline and even amorphous or glassy materials is the direct measurement of translational Li jumps via stimulated echoes. The so-called spin-alignment echo (SAE) technique was developed for deuterons (spin-1 nuclei) by Spiess [16] and recently applied also to spin-3/2 quadrupole nuclei like ^{9}Be [17–19] and ^{7}Li [20–25] with quadrupole coupling constants similar to that of deuterons. The method gives direct access to extremely slow cation exchange rates on the kHz to sub-Hz timescale, as was quite recently demonstrated by us in a comprehensive NMR study about Li dynamics in layer-structured Li_xTiS_2 [26]. Moreover, the evolution time dependence of final state amplitudes of stimulated echo correlation functions contains information about geometric parameters of the diffusion pathway [27].

In the present paper polycrystalline lithium orthosilicate, Li_4SiO_4, serves as a model substance for the demonstration of stimulated-echo NMR spectroscopy to be, besides 2D exchange MAS NMR, an additional tool for the direct investigation of Li dynamics in crystalline ion conductors. Li dynamics in Li_4SiO_4 has already been probed by 2D NMR by Xu *et al* [8]. Additionally, the lithium cation exchange process between different crystallographic sites in Li_4SiO_4 was previously observed by Stebbins *et al* [28] via recording temperature dependent 1D ^{6}Li MAS spectra. ^{7}Li spin–lattice relaxation NMR measurements on Li_4SiO_4 and related materials were carried out by Smaihi *et al* [29, 30]. The presence of a relatively large number of electrically inequivalent sites, being occupied by Li cations, makes the material an interesting model substance for ^{7}Li SAE NMR. In Li_4SiO_4, 56 Li ions are distributed among 126 available Li sites. In agreement with the results on the crystal structure [31], high-resolution ^{6}Li MAS NMR data indicate four different LiO_n polyhedra with $n = 3, 4, 5, 6$ in Li_4SiO_4 [8, 28]. It is most likely that all Li ions participate in the diffusion process.

Up to now, crystalline as well as glassy Li_4SiO_4-based compounds [32–34] have been investigated with regard to their use as solid electrolytes in secondary Li batteries. Additionally, Li_4SiO_4 has attracted considerable interest as a possible solid breeder material for fusion reactors [35, 36]. Furthermore, concerning greenhouse gases in the atmosphere, Li_4SiO_4 [37] and metal doped Li_4SiO_4 compounds [38] are expected to be the future prime materials to serve as CO_2 absorbents.

2. Spin-alignment echo (SAE) NMR

Spin-alignment echo NMR spectroscopy probes Li diffusion, simply put, by labelling the ions via their angular quadrupole frequency ω_Q, which is due to the interaction between the nuclear quadrupole moment and a non-vanishing electric field gradient (EFG) tensor at the site of the nucleus. Different crystallographic and thus electrically distinct Li sites are characterized by different quadrupole frequencies. Jumping of the ion between these sites leads to a time dependence of ω_Q, which can be used to 'count' ionic jumps as a function of observation time. Using common notation, see e.g. [39], the quadrupole Hamiltonian is given by

$$\hat{H}_Q = \frac{1}{\sqrt{6}}\omega_Q \hat{T}_{20} \tag{1}$$

with the spherical tensor operator $\hat{T}_{20} = \frac{1}{\sqrt{6}}[3\hat{I}_z^2 - I(I+1)]$ and the quadrupole frequency

$$\omega_Q/2\pi = \tfrac{1}{4} C_Q \left(3\cos^2\Theta - 1 - \eta\sin^2\Theta\cos(2\Phi)\right) \tag{2}$$

where $C_Q = e^2qQ/h$ is the quadrupole coupling constant with the proton charge e, h is Planck's constant and Q is the electric quadrupole moment of the nucleus. eq is the principal component of the EFG. η denotes the asymmetry parameter of the quadrupole interaction. The polar angles Θ and Φ determine the orientation of the external field B_0 in the principal axis system of the EFG tensor at the nuclear site. The quadrupole interaction alters the angular Zeeman frequency ω_0 according to $\omega_0 \pm \omega_Q$. Provided electrically inequivalent sites are visited by the jumping ion, the information about the dynamic process is coded in terms of a temporal change in ω_Q.

The spin-alignment technique allows one to measure directly a single-particle correlation function yielding information about dynamic as well as geometric parameters of the hopping process. Its analogy to quasielastic neutron scattering, operating on a much shorter timescale, was pointed out in [40, 41], for example. The radio frequency pulse sequence used to sample spin-alignment echoes is based on the three-pulse method of Jeener and Broekaert [42]

$$\beta_{1_{\phi_1}} - t_p - \beta_{2_{\phi_2}} - t_m - \beta_{3_{\phi_3}} - t$$

with $\beta_1 = 90°$ and $\beta_2 = \beta_3 = 45°$, ϕ_i denote the phase of the respective pulse. Starting from thermal equilibrium $\hat{I}_z = \hat{T}_{10}$, the first two pulses generate, if $|\phi_1 - \phi_2| = 90°$, a quadrupolar alignment state according to [27]

$$\hat{T}_{10} \xrightarrow{\beta_1\hat{I}_{\phi_1}, \hat{H}_Q t_p, \beta_2\hat{I}_{\phi_2}} -\tfrac{1}{2}\sqrt{\tfrac{3}{2}}\sin\beta_1\sin 2\beta_2\sin(\omega_Q t_p)\hat{T}_{20}. \tag{3}$$

The reading pulse transforms spin alignment back into an observable transverse coherent magnetization leading to an echo at $t = t_p$. If the last pulse is an X pulse, a magnetization along the x-axis is observed:

$$-\tfrac{1}{2}\sqrt{\tfrac{3}{2}}\sin\beta_1\sin 2\beta_2\sin(\omega_Q t_p)\hat{T}_{20} \xrightarrow{\beta_3\hat{I}_{\phi_3}, \hat{H}_Q t} \tfrac{9}{20}\sin\beta_1\sin 2\beta_2\sin 2\beta_3\sin(\omega_Q t_p)\sin(\omega_Q t). \tag{4}$$

With $\beta_1 = 90°$ and $\beta_2 = \beta_3 = 45°$ the echo amplitude S_2' is maximal and given by [27]

$$S_2'(t_p, t_m, t) = \tfrac{9}{20}\langle\sin[\omega_Q(0)t_p]\sin[\omega_Q(t_m)t]\rangle. \tag{5}$$

Angular brackets $\langle\cdots\rangle$ denote the powder average. For fixed t_p the decay of the alignment echo

amplitude $S_2'(t_p, t_m)$ with increasing mixing time t_m is directly due to successful jumps of the ions between Li sites with different quadrupole frequencies. Usually this decay step follows an exponential function $S_2' \propto e^{-(t_m/\tau_{SAE})^{\gamma_\tau}}$ with $0 < \gamma_\tau \leqslant 1$ and a time constant τ_{SAE}, being in the ideal case equal to the motional correlation time. Additionally, echo formation will be affected by the decay of the spin-alignment state due to spin–lattice relaxation processes. This additional echo damping can be taken into account by a second exponential, so that the complete curve is given by $S_2 = S_2' \cdot e^{-(t_m/T_{1SAE})^{\gamma_T}}$ with the corresponding stretching exponent γ_T generally ranging between $0 < \gamma_T \leqslant 1$. If a pure spin-alignment state was created, T_{1SAE}^{-1} equals the quadrupolar relaxation rate T_{1Q}^{-1}, which determines the lower limit of the experimental time window to investigate ionic motions, i.e., $\tau_{SAE}^{-1} > T_{1Q}^{-1}$ must hold.

Experimentally, in the case of ^{7}Li, being subject to relatively strong dipole–dipole interactions as compared to, e.g., ^{9}Be, the complete suppression of dipolar (D) order simultaneously with quadrupolar (Q) order is difficult to realize even at very small evolution times t_p [22, 23]. The two corresponding time constants $\tau_{SAE,D}$ and $\tau_{SAE,Q}$ determining the echo decay will normally differ by about a factor of two, if at all (cf, e.g., an analogous NMR relaxation study in [43], where the influence of dipolar and quadrupolar contributions on the diffusion induced relaxation rate of polarized radioactive ^{8}Li nuclei was investigated in pure Li metal and Li alloys, respectively). Whereas pure SAE NMR leads directly to a single-particle correlation function, the decay of dipolar order is described at least by a two-particle correlation function.

3. Experimental details

^{7}Li NMR measurements on Li_4SiO_4 (delivered by Alfa Aesar, purity 99.9%, −100 mesh powder) were mostly performed at Larmor frequencies $\omega_0/2\pi$ of 155.5 and 77.8 MHz, corresponding to external magnetic fields B_0 of 9.4 and 4.7 T, respectively. Additionally, some NMR experiments were done at 39.1 MHz. The measurements at 9.4 T were carried out on a Bruker MSL 400 spectrometer combined with a shimmed Oxford cryomagnet of higher field homogeneity. For the experiments at lower magnetic fields a modified Bruker MSL 100 spectrometer connected to a tunable Oxford cryomagnet was used. Temperatures were monitored in both cases by means of an Oxford ITC4 unit with an accuracy of ±1 K in both cases. The $\pi/2$ pulse length was about 4 μs (250 kHz bandwidth), ensuring a non-selective excitation of both the central and the satellite contributions to the NMR signals. For the measurements below 473 K standard probes designed by Bruker were employed. NMR spectra at higher temperatures were recorded using a home-built high-temperature probe working at temperatures up to about 1100 K.

^{7}Li spin-alignment echoes as a function of mixing (t_m) and preparation time (t_p) were recorded using the three-pulse sequence of Jeener and Broekaert: $(\pi/2)_y$–t_p–$(\pi/4)_x$–t_m–$(\phi)_y$–t–acquisition (acq.). In order to maximize the echo signal, the last pulse was chosen to be a $\pi/4$ pulse [23]. Extensive phase cycling was employed in order to suppress unwanted coherences and to reduce undesirable effects of imperfect radio frequency pulses [23, 27]. If not stated otherwise, the preparation time was chosen to be 10 μs. ^{7}Li solid-echo spectra were recorded using the sequence $(\pi/2)$–t_e–(64°)–t–aqc. Since ^{7}Li is a spin-3/2 nucleus a refocusing pulse of 64° is used in order to obtain the correct intensity ratio for the central and satellite transitions [44]. The interpulse delay time t_e was chosen between 10 and 20 μs. Relaxation rates were measured using the standard saturation recovery technique; i.e., a series of $(\pi/2)$ pulses was used to destroy any longitudinal magnetization M and the subsequent recovery of M was detected after variable delay times t_{delay}. Magnetization transients $M(t_{delay})$ were obtained by plotting the area under the free induction decays as a function of t_{delay}.

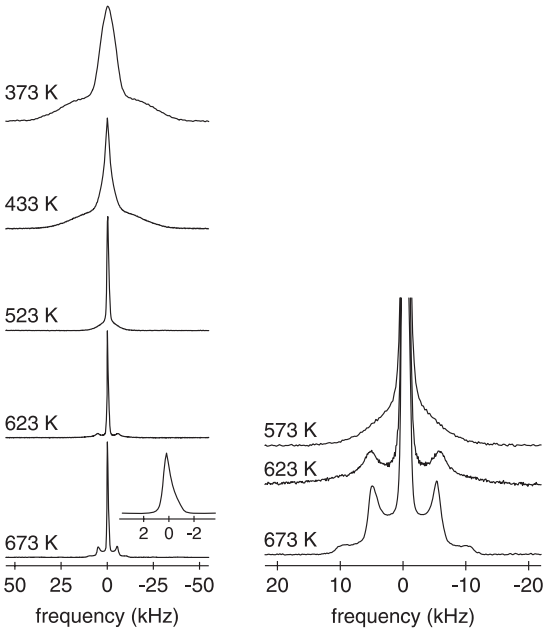

Figure 1. Left: evolution of ^{7}Li solid echo NMR spectra (155.5 MHz) of lithium orthosilicate with increasing temperature. The inset shows the central transition only, indicating its anisotropy at 673 K. Right: magnification of the spectra partly shown on the left-hand side, too. At higher temperatures a well defined axially symmetric quadrupolar powder pattern with a final quadrupole coupling constant of 21(1) kHz emerges.

4. Results and discussion

4.1. Solid-echo and spin-alignment spectra

First insights into Li dynamics in polycrystalline Li_4SiO_4 were obtained by recording ^{7}Li NMR spectra as a function of temperature. Figure 1 presents some selected ^{7}Li NMR solid-echo spectra at temperatures between 373 and 673 K. In the dynamic regime of the rigid lattice, i.e., below 350 K, the NMR lines are composed of a central line with a width (full width at half maximum) of about 10 kHz and a Gaussian shaped quadrupole contribution with a width of about 50 kHz. It reflects the distribution of electric field gradients (EFGs) in the material due to different crystallographic Li sites. Both contributions are dipolarly broadened. Line narrowing of the central transition, caused by averaging of local magnetic fields due to Li hopping, i.e. motional narrowing, starts at about 370 K. At this temperature the mean Li jump rate is expected to be of the order of 10^{-3} s, indicating the poor Li diffusivity of Li_4SiO_4 at this temperature. This fact makes the material a suitable model substance for the study of extremely slow Li motions via spin-alignment echo NMR. At intermediate temperatures, e.g. at 433 K, the central line of the static NMR spectrum is partially narrowed. It is composed of a broad Gaussian and a narrow Lorentzian line. Such a partial motional narrowing indicates a distribution of Li jump rates in Li_4SiO_4. At about 600 K narrowing of the central part is completed and the jump rate τ^{-1} of Li^+ is expected to be several times larger than the rigid-lattice line width, i.e., τ^{-1} presumably takes values between 10^5 and 10^6 s^{-1}. For further illustration, the broadening of the central line due to dipolar interactions is shown in figure 2 versus temperature T. High-temperature data were recorded at a magnetic field of 4.7 T with a

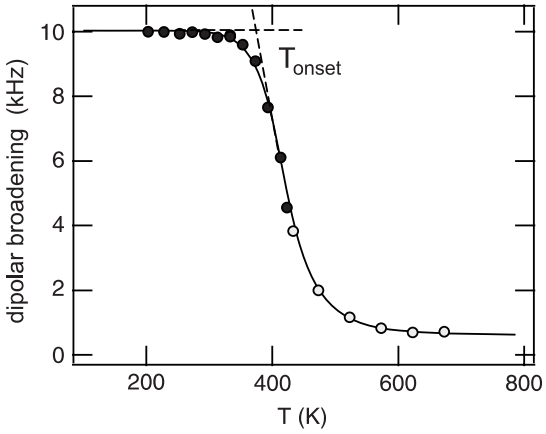

Figure 2. Dipolar broadening of the ^{7}Li NMR central transition of Li_4SiO_4. Onset of NMR line narrowing sets in at $T_{onset} \approx 370$ K. Data were obtained at 155.5 MHz (●) and 77.8 MHz (○), respectively. The solid line is just to guide the eye.

home-built probe, whereas the low-T data of figure 2 were recorded at 9.4 T using a commercial Bruker probe.

Besides magnetic interactions, the jumping ions experience fluctuating site specific electric interactions. Sufficiently fast cation jumps between sites with different EFGs result in an averaging of electric quadrupole interactions. Regarding the ^{7}Li spectra of figure 1 it can be clearly seen that the width and the intensity of the broad quadrupole part is reduced with increasing temperature. However, even at very high temperatures the quadrupole interactions are not completely averaged due to Li diffusion. A definite quadrupole powder pattern with a small quadrupole coupling constant of about 21 kHz emerges and distinctly shows up at 673 K. It is further noted that the central line is anisotropically broadened at very high temperatures. Both observations point to the anisotropy of Li motion caused by the finite number of, say four, inequivalent Li sites being present in crystalline Li_4SiO_4. Such an effect was also found in lithium thioborate sulfides by Grüne *et al* [45], for example.

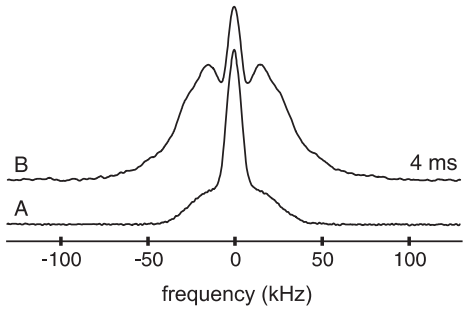

Figure 3. Comparison of a typical ^{7}Li solid-echo (A) powder spectrum with the corresponding spin-alignment (B) powder spectrum ($t_p = 10$ μs, $t_m = 4$ ms) at 373 K of Li_4SiO_4. Note the increased intensity of the satellite contributions for the spin-alignment spectrum.

In figure 3 the ^{7}Li solid-echo NMR spectrum at 373 K is exemplarily compared to that obtained with the spin-alignment three-pulse sequence using a short evolution time of

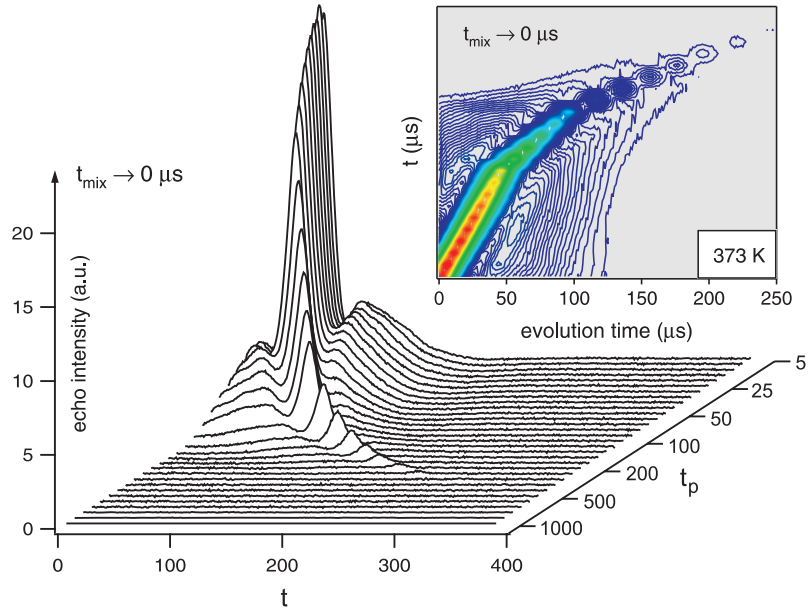

Figure 4. Evolution time dependence of spin-alignment echoes recorded at a Larmor frequency of $\omega_0/2\pi = 155.5$ MHz for a short mixing time $t_m \rightarrow 0\ \mu$s. The echoes were measured at $T = 373$ K.

$t_p = 10\ \mu$s. Both spectra were recorded at 155.5 MHz. All the spin-alignment spectra show an enhanced intensity of the quadrupolar satellite contributions at short evolution times, whereas, at first glance, the intensity of the central contribution around $\omega_0/2\pi = 155.5$ MHz is reduced. A pure spin-alignment spectrum would be composed of satellite transitions only. However, it has recently been shown by simple spectrum modelling that homonuclear dipolar coupling of ^{7}Li nuclei generates signal intensities near the Larmor frequency $\omega_0/2\pi$ for each satellite transition [22]. In the case of a powder spectrum these additional intensities are added up and appear as a 'central' line in the spin-alignment spectrum. A possible phase shift of these contributions depends on the radio frequency offset and on the length of the reading pulse of the Jeener–Broekaert sequence [23]. Nevertheless, when comparing solid-echo and spin-alignment spectra, the latter are dominated by quadrupole contributions, indicating that the phase information $\sin\omega_{Q_i}(t_m)t_p$ is mainly stored in the $\hat{T}_{20}$ state after the first $\pi/4$ pulse of the JB sequence. This is the case when short evolution times t_p are used (see below). Longer evolution times will increase the portion of dipolar contributions to the stimulated echo spectra. Furthermore, in contrast to the solid-echo spectrum, the quadrupole part of the spin-alignment spectrum is slightly structured. It is composed of at least three different subspectra due to the different crystallographic sites in Li_4SiO_4. Subspectra corresponding to sites being less populated by Li ions will contribute to the alignment spectrum, too, but they will certainly not dominate the line shape.

Spin-alignment spectra were obtained by Fourier transformation of the corresponding echoes beginning from the echo top at $t = t_p$. A series of stimulated echoes is shown in figure 4 for various evolution times t_p. The contour plot of figure 4 reveals the intensities of the different contributions to the stimulated echoes. They firstly comprise the 'spin-alignment echo' as the main echo intensity, which appears exactly at $t = t_p$ and which contains the quadrupole information stored at $t = t_m$ in the alignment state $\hat{T}_{20}$. Near $t = t_p$ further intensities show up

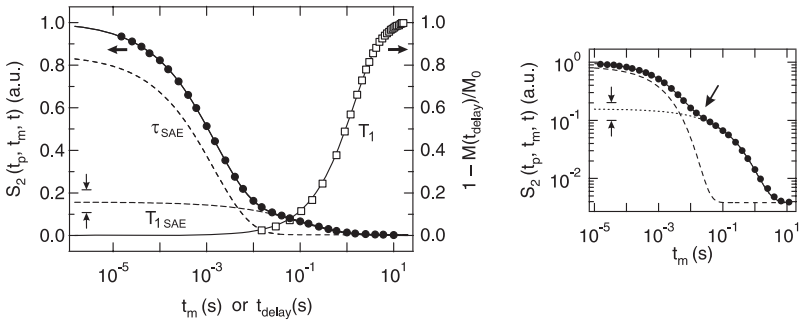

Figure 5. Left: semilog plot of a typical S_2-decay in Li_4SiO_4 recorded at 155.5 MHz and 373 K. The solid line represents a fit using equation (6) and yields $\tau_{SAE} = 1.5(1) \times 10^{-3}$ s and $\gamma_\tau = 0.57$. The overall fit (solid line) is composed, according to equation (6), of the two stretched exponentials displayed as dashed and dotted lines, respectively. A plateau value S_∞ of 0.16(1) indicates the participation of a relatively large number of Li sites in the diffusion process. Moreover, the (normalized) recovery of longitudinal magnetization with increasing delay time t_{delay}, proceeding on a much longer timescale as compared to the echo decay, is shown for comparison with the second decay step of S_2. Right: log–log representation of the correlation function in order to expose its two-step behaviour (see arrow).

at acquisition times t longer and even shorter than t_p. Fourier transformation (FT) of the fast decaying main echo yields the satellite intensities of the corresponding spectrum, whereas the intensities at larger acquisition times refer to dipolar contributions to the spectrum (see above), which appear close to the Larmor frequency as a 'central' line, as mentioned above. In order to obtain hopping correlation functions for a fixed evolution time t_p and as a function of mixing time t_m (see section 4.2), the amplitudes of the echoes were read out at $t = t_p$, i.e. at the top of the stimulated echo. As can be clearly seen from figure 4, the shorter the t_p that is chosen, the more intense the spin-alignment contribution to the echo will be and, thus, the larger the satellite intensities in the corresponding spectra after subsequent FT will become, cf also [17]. Therefore, SAE correlation functions were recorded at very short t_p. If not stated otherwise, the evolution time was chosen to be 10 μs.

4.2. Two-time spin-alignment correlation functions

Li jump rates in polycrystalline Li_4SiO_4 were studied by recording spin-alignment echoes at fixed t_p and as a function of mixing time t_m. The latter was varied over several decades, i.e. from 10 μs to 100 s. SAE NMR experiments were performed between 300 and 433 K, thus mainly in the dynamic regime of the rigid lattice where extremely slow Li motions are expected with jump rates being smaller than 10^3 s^{-1}. In figure 5 a typical decay of the echo amplitude S_2 as a function of mixing time t_p is shown. The obtained decay curve $S_2(t_p, t_m, t)$, normalized to the range from zero to unity, was recorded at a frequency of 155.5 MHz and at $T = 373$ K. It is composed of two stretched exponentials and can be well fitted (solid line in figure 5) with equation (6) in order to extract the decay constant τ_{SAE}:

$$S_2(t_p, t_m, t) = (A e^{-(t_m/\tau_{SAE})^{\gamma_\tau}} + B) \cdot e^{-(t_m/T_{1SAE})^{\gamma_T}}. \quad (6)$$

The second exponential is presumably due to the influence of (quadrupolar) longitudinal relaxation on the echo decay. The time constant of this process is called T_{1SAE} here. T_{1SAE} is expected to be orders of magnitude larger than τ_{SAE} corresponding to the first decay step, which is assumed to be directly induced by changes of ω_Q due to slow Li jumps, i.e. $T_{1SAE} \gg \tau_{SAE}$. At 373 K, for instance, the decay rate τ_{SAE}^{-1} is 670(10) s^{-1}; the respective

stretching exponent is about 0.6, indicating a distribution of jump rates in Li_4SiO_4. Such a distribution of jump rates was previously observed also by 2D exchange NMR. The SAE stretching exponent γ_τ decreases from 0.7 to 0.4 with the temperature increasing from 300 to 433 K. This decrease may be the consequence of residual dipolar contributions being more and more averaged with increasing temperature. Stebbins *et al* [28] estimated a mean Li jump rate of 300(100) s^{-1} at about 360 K by analysing the temperature dependence of ^{6}Li MAS NMR spectra. At this temperature the alignment echo decay follows a stretched exponential with $\tau_{SAE}^{-1} = 380(10)\ s^{-1}$. Thus, τ_{SAE}^{-1} can be identified here with the mean Li jump rate τ^{-1}. ^{6}Li spectra show four different resonance lines due to the different Li sites in Li_4SiO_4. Coalescence of these NMR lines into a single line is observed when the mean residence time of the Li ions becomes smaller than the inverse frequency distance between the outer resonances of the ^{6}Li spectrum.

The plateau value, $S_\infty = A/(A + B)$, being related to the number of inequivalent sites visited by the jumping ion while diffusing, is about 0.16. Usually, S_∞ has to be recorded at sufficiently large evolution times [41]. However, in the present case even at a very short evolution time the value $1/S_\infty \approx 6$ indicates already a relatively large but finite number of electrically inequivalent sites participating in the diffusion process. For short evolution times ($t_p < 20\ \mu s$) the plateau value S_∞ ranges from 0.14(2) to about 0.23(2) between $T = 333$ and 433 K. The latter value gives rise to the assumption that four different Li sites are involved in the diffusion process. In fact, exactly four different Li polyhedra LiO_n ($n = 3, 4, 5, 6$) are present in Li_4SiO_4. Therefore, we conclude that all Li sites participate in the transport process. It has to be mentioned that S_∞ might be affected by the number of dipolarly coupled Li spin-pairs [22]. The larger the number of effectively coupled Li spins is, the lower is the final state amplitude. However, at $T = 433$ K the central line of the solid-echo spectrum is already somewhat narrowed, so that dipolar interactions become partially averaged at this temperature. Thus at 433 K a final state amplitude is found whose value is comparable to the one which would be obtained when dipolar interactions were completely absent.

Additionally, we have analysed two-time correlation functions recorded at $t = t_p = 10\ \mu s$, but which were obtained by plotting the amplitude of the stimulated echo at $t = t_p + t' = 50\ \mu s$ versus t_m [46]. Between 293 and 413 K the corresponding decay constants were larger by a factor of two when compared to those obtained at $t = t_p$. This difference is expected if one assumes that the SAE-curve sampled at $t = t_p$ represents a *single*-particle correlation function, whereas the other one being read out at larger acquisition times $t_p + t'$ accounts for dipolar contributions leading to a *two*-particle hopping correlation function (at least), as mentioned above. This is corroborated by the observation that the final state amplitudes of the latter correlation functions are reduced by a factor of two [46].

As mentioned above, the second decay step, leading from the final state amplitude S_∞ at intermediate mixing times to $S_0 = 0$ is primarily due to longitudinal relaxation and does not necessarily reflect a slower diffusion process in Li_4SiO_4. Such a slow jump process would be difficult to detect because of the influence of spin–lattice relaxation which starts to affect the echo decay considerably at mixing times larger than 0.01 s (cf figure 3). The lower limit of detectable jump rates via stimulated echoes is given by the quadrupolar relaxation rate T_{1Q}^{-1} (see above), whereas the upper limit is determined by the spin–spin relaxation rate T_2^{-1}, thus $T_2^{-1} > \tau_{SAE}^{-1} > T_{1Q}^{-1}$ should hold. T_2^{-1} is of the order of $10^{-4}\ s^{-1}$ in the rigid lattice regime. T_{1Q} either equals or is smaller than T_1. In order to demonstrate on which timescale T_1 relaxation proceeds in comparison with the timescale of the first and second decay steps, the recovery of longitudinal magnetization is shown in figure 5, too. Blank squares show the recovery of $M(t_{delay})$ as measured independently via saturation recovery experiments at the same radio frequency. In the present case we have $T_{1SAE} = T_{1Q} \approx 0.3 \cdot T_1$.

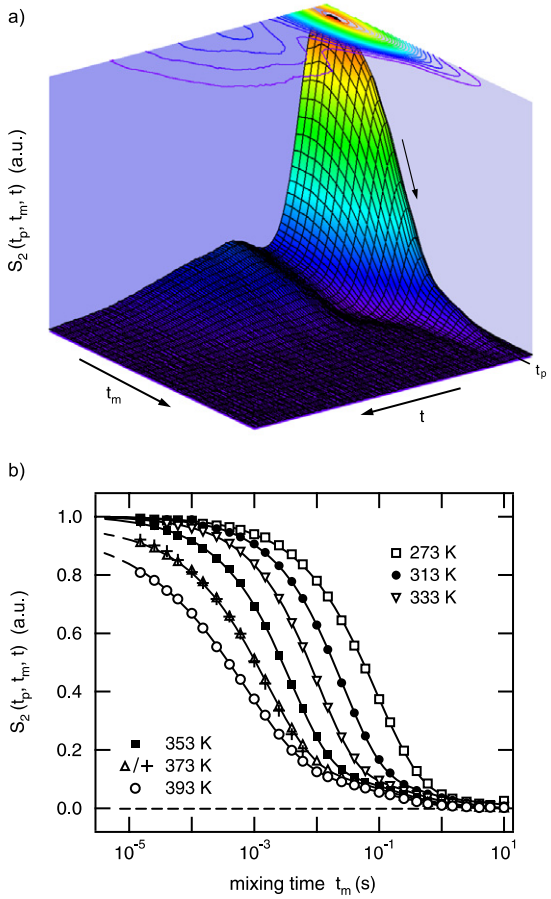

Figure 6. (a) Evolution of stimulated echoes as a function of mixing time t_m and acquisition time t. Data were recorded at fixed evolution time $t_p = 10\ \mu s$, $\omega_0/2\pi = 155.5$ MHz and $T = 373$ K. The spin-alignment echo maximum appears at $t = t_p$. (b) Spin-alignment echo decay curves (semilog plot) for variable temperatures as a function of t_m and fixed $t_p = 10\ \mu s$. The frequency was 155.5 MHz; the same results were obtained for 77.8 MHz above room temperature. As an example, echo amplitudes (+) at 373 K recorded at 77.8 MHz are shown for comparison with data at 373 K and 155.5 MHz (△). The echo amplitude was read out at the echo top, i.e. at $t = t_p$. With increasing temperature the inflexion point of the respective curves is shifted to smaller mixing times t_m, resulting in smaller values of τ_{SAE}.

4.3. ^{7}Li SAE decay rates — comparison with results from other NMR techniques

Spin-alignment echo decay curves for various temperatures in the range 273–393 K are shown in figure 6. The curves were fitted using equation (6) in order to extract the jump rates τ_{SAE}^{-1} via the echo decay. In figure 7 the corresponding (mean) decay rates are shown in an Arrhenius representation. They show thermally activated behaviour representing extremely slow Li diffusion with an activation energy of 0.53(1) eV. The decay rates τ_{SAE}^{-1} above room temperature are independent of the radio frequency $\omega_0/2\pi$ as expected for a motional correlation rate. In contrast to this, the T_1^{-1} rates do depend on the resonance frequency. Spin-alignment decay rates and spin–lattice relaxation rates were recorded at two resonance frequencies which differ by a factor of two (cf figure 7) to illustrate this dependence.

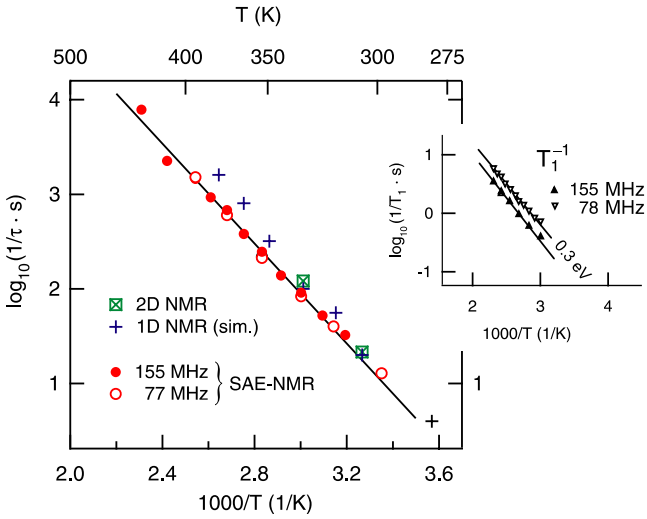

Figure 7. Temperature dependence of the ^{7}Li spin-alignment decay rates τ_{SAE}^{-1} recorded for fixed evolution time $t_p = 12\ \mu$s. Decay rates were recorded at two different frequencies of 77.8 MHz (○) and 155.5 MHz (●). In contrast to the independently measured ^{7}Li NMR spin–lattice relaxation rates at these resonance frequencies (see the inset) the spin-alignment decay rates are frequency independent. The τ_{SAE}^{-1} values are compared with Li jump rates (⊠), which, by ^{6}Li 2D exchange MAS NMR, were directly recorded at two different temperatures by Xu *et al* [8]. The simulated (sim.) data (+) were also taken from [8]. They were obtained by analysing temperature dependent 1D MAS NMR spectra of ^{6}Li nuclei.

For comparison, in figure 7 the jump rates obtained directly by using 2D exchange NMR experiments by Xu *et al* [8] are shown, too. Furthermore, exchange rates, taken again from [8], which had been derived by a peak shape simulation of experimental 1D ^{6}Li MAS NMR spectra, are displayed. The latter rates were obtained assuming a random-walk model and the participation of all cation sites in the diffusion process. The spin-alignment values agree with these two sets of previous results. The 2D exchange rates were recorded at two temperatures only, namely at 306 and 332 K. Furthermore, 2D NMR spectra were monitored within a rather small range of mixing times as compared to that used in the SAE NMR measurements here (cf figure 6). The two τ^{-1} values recorded by ^{6}Li 2D NMR spectra represent the sum of exchange rates between four pairs of different LiO_n polyhedra in Li_4SiO_4, namely cation exchange between LiO_4 and LiO_3, LiO_4 and LiO_6, LiO_5 and LiO_6, as well as between LiO_3 and LiO_6. Li exchange between LiO_4 and LiO_5 polyhedra are difficult to detect by 2D NMR due to overlapping cross-peaks. However, the $LiO_4 \leftrightarrow LiO_5$ exchange rate seems to be negligible in comparison with the other exchange rates. Whereas by 2D exchange NMR Li hopping rates and activation energies between selected pairs of LiO_n polyhedra can be measured, by SAE NMR overall exchange rates are obtainable, i.e. even those jumps are 'visible' which cannot be detected via an exchange NMR experiment due to limited resolution. Therefore, also Li jumps between temporarily occupied Li sites and regular LiO_n polyhedra may contribute to the spin-alignment decay, provided a change of ω_Q is associated with these translational motions. Direct jumps between sites with the same local symmetry are invisible for SAE NMR as ω_Q does not change. However, the comparison with the 2D NMR results by Xu *et al* [8] shows that such a 'self-exchange process' seems to be negligible for Li_4SiO_4. In Li_4SiO_4 only edge-sharing polyhedra exist. Thus, in view of the good agreement between results obtained by SAE and 2D NMR, one may conclude that Li jumps occur directly between edge-shared polyhedra, only.

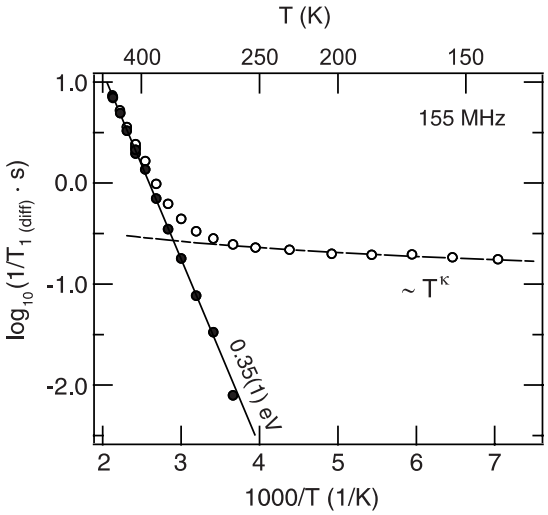

Figure 8. Temperature dependence of the spin–lattice relaxation rates T_1^{-1} (○) measured at 155.5 MHz between 140 and 450 K. The non-diffusive relaxation rates following the temperature dependence T^{κ} with $\kappa = \frac{1}{2}$ were extrapolated to higher T and subtracted from T_1^{-1} to obtain the purely diffusion induced rates $T_{1\mathrm{diff}}^{-1}$ (●). The solid line corresponds to an activation energy of about 0.35 eV.

Diffusion pathways involving a temporary occupation of sites connecting two LiO_n polyhedra do not seem to be favoured. This is in agreement with an early speculation that in Li_4SiO_4 edge-shared polyhedra might provide the easiest diffusion pathways with the lowest activation energies [47].

The activation energy for Li diffusion in Li_4SiO_4, weighted averaged from the two 2D NMR spectra, was estimated to be about 0.7 eV [8]. The activation energy determined by analysing 1D ^{6}Li MAS NMR spectra is about 0.56 eV [8], and thus in nice agreement with the value of 0.53(1) eV from SAE NMR obtained here. In contrast to these results, the activation energy deduced from the low-T flank of the diffusion induced peak of the spin–lattice relaxation rate T_1^{-1}, which is shown in figure 8, is much lower. The low-T flank can be detected in the same temperature range in which the SAE NMR correlation functions were recorded. Regarding the overall temperature dependence of T_1^{-1} two regimes can be discerned (cf figure 8). Below room temperature only a non-diffusive and weakly temperature dependent background relaxation rate is measured. In this region T_1^{-1} is proportional to T^{κ} with $\kappa = \frac{1}{2}$. Presumably, the relaxation rate is induced by paramagnetic impurities. Above room temperature the spin–lattice relaxation rate is increasingly influenced by ionic diffusion. Partly, the low-T flank of the diffusion induced peak shows up. The relaxation rates T_1^{-1} shown in figure 8 were obtained by fitting the magnetization transients $M(t_{\mathrm{delay}})$ with a stretched exponential function. The corresponding stretching exponent, which should not be mixed with that of SAE NMR, varies between 0.7 and 0.9 and shows a minimum at about 400 K. This behaviour may be interpreted in the following way. At low temperatures the influence of non-diffusive relaxation mechanisms is masking the deviation from monoexponential relaxation being expected for ^{7}Li with $I = 3/2$ (see below), whereas at higher temperatures, due to the increased Li diffusivity, a common spin temperature is being established, which leads to less stretched magnetization curves. Alternatively, the transients can be fitted (somewhat better) with a double-exponential function. The two corresponding spin–lattice relaxation times obey

the relation $T_1' \approx \frac{1}{3}T_1''$. Thus, both values show the same temperature dependence. In general, for the quadrupole nucleus ^{7}Li two-exponential time behaviour is expected provided not all the nuclei are exposed to the same spin temperature as is the case in the extreme-narrowing regime [43, 48], i.e. above 500 K in the present case (cf figure 2).

In order to obtain the purely diffusion induced relaxation rate $T_{1\mathrm{diff}}^{-1}$, the background rates of figure 8 were extrapolated to higher temperatures and subsequently subtracted from the total spin–lattice relaxation rate T_1^{-1}. Plotting $T_{1\mathrm{diff}}^{-1}$ versus $1/T$ reveals an apparent activation energy of about 0.35(1) eV, i.e., less than those measured by exchange and SAE NMR. If the correction for the background rates is not applied an activation energy of about 0.3 eV is obtained, cf the inset of figure 7. Obviously, the slope of the low-T flank is influenced by correlation effects and deviates from standard behaviour as often found in structurally complex or disordered ionic conductors; see, e.g., [13–15]. The diffusion induced rate maximum will show up at much higher temperatures [30], outside the range covered here by spin–lattice relaxation measurements. There is evidence from conductivity measurements that above 573 K the number of mobile ions becomes temperature dependent due to the formation of Frenkel defects in the structure [30]. Thus, a straightforward comparison of the low-temperature data presented here, with results about Li dynamics at much higher temperatures is not possible. High-temperature NMR relaxation data [30] and conductivity measurements [30, 49, 50] indicate that the diffusion mechanisms change upon heating.

5. Conclusion

We have investigated the low-temperature (300–450 K) Li dynamics in polycrystalline Li_4SiO_4 by means of ^{7}Li spin-alignment echo (SAE) NMR spectroscopy. Using very short evolution times we have recorded two-time hopping correlation functions and were able to measure directly, i.e. without involving a theoretical model, extremely slow Li jumps with rates in the Hz to kHz range. Independent of the nucleus under investigation the exchange rates are in good agreement with those obtained previously by 1D ^{6}Li and 2D ^{7}Li exchange MAS NMR experiments on polycrystalline Li_4SiO_4. Apart from 2D exchange NMR, there exists no other experimental method to measure such extremely slow Li motions directly. Relatively large SAE final state amplitudes give rise to the assumption that all Li sites participate in the diffusion process, as was already found by 2D NMR. The good agreement of the results obtained by the two methods shows that Li SAE NMR is able to complement earlier developed, but rarely used techniques for the measurement of microscopic Li diffusion parameters. The advantage of SAE NMR over 2D exchange NMR experiments is that stimulated echo NMR is applicable to a much broader class of Li containing materials. It might become a time-saving alternative to Li exchange NMR experiments.

Acknowledgment

We would like to thank the Deutsche Forschungsgemeinschaft (DFG) for financial support.

References

[1] Tarascon J-M and Armand M 2001 *Nature* **414** 359
[2] Whittingham M S 2004 *Chem. Rev.* **104** 4271
[3] Grey C P and Dupré N 2004 *Chem. Rev.* **104** 4493
[4] Brinkmann D 1992 *Prog. Nucl. Magn. Reson. Spectrosc.* **24** 527
[5] Müller-Warmuth W and Schöllhorn R 1994 *Progress in Intercalation Research* (Dordrecht: Kluwer)

[6] Heitjans P, Indris S and Wilkening M 2005 Solid-state diffusion and NMR *Diffusion Fundamentals* ed J Kärger, F Grinberg and P Heitjans (Leipzig: Leipziger Universitätsverlag) p 226
Heitjans P, Indris S and Wilkening M 2005 *Diffus. Fundam.* **2** 45 http://www.uni-leipzig.de/diffusion/journal/pdf/volume2/diff_fund_2(2005)45.pdf
[7] Heitjans P, Schirmer A and Indris S 2005 NMR and β-NMR studies of diffusion in interface-dominated and disordered solids *Diffusion in Condensed Matter—Methods, Materials, Models* ed P Heitjans and J Kärger (Berlin: Springer)
[8] Xu Z and Stebbins J F 1995 *Science* **270** 1332
[9] Verhoeven V W J, de Scheper I M, Nachtegaal G, Kentgens A P M, Kelder E M and Mulder F M 2001 *Phys. Rev. Lett.* **86** 4314
[10] Cabana J, Dupré N, Rousse G, Grey C P and Palacn M R 2005 *Solid State Ion.* **176** 2205
[11] Cahill L S, Chapman R P, Britten J F and Goward G R 2006 *J. Phys. Chem.* B **110** 7171
[12] Bork D and Heitjans P 2001 *J. Phys. Chem.* B **105** 9162
[13] Meyer M, Maass P and Bunde A 1993 *Phys. Rev. Lett.* **71** 573
[14] Ngai K L 1980 *Commun. Solid State Phys.* **5** 141
[15] Funke K 1993 *Prog. Solid State Chem.* **22** 111
[16] Spiess H W 1980 *J. Chem. Phys.* **72** 6755
[17] Tang X-P and Wu Y 1998 *J. Magn. Reson.* **133** 155
[18] Tang X-P, Busch R, Johnson W L and Wu Y 1998 *Phys. Rev. Lett.* **81** 5358
[19] Tang X-P, Geyer U, Busch R, Johnson W L and Wu Y 1999 *Nature* **402** 160
[20] Böhmer R, Jörg T, Qi F and Titze A 2000 *Chem. Phys. Lett.* **316** 419
[21] Qi F, Jörg T and Böhmer R 2002 *Solid State Nucl. Magn. Reson.* **22** 484
[22] Qi F, Diezemann G, Böhm H, Lambert J and Böhmer R 2004 *J. Magn. Reson.* **169** 225
[23] Qi F, Rier C, Böhmer R, Franke W and Heitjans P 2005 *Phys. Rev.* B **72** 104301
[24] Wilkening M and Heitjans P 2005 *Defect Diffus. Forum* **237–240** 1182
[25] Wilkening M and Heitjans P 2005 *Diffus. Fundam.* **2** 60 http://www.uni-leipzig.de/diffusion/journal/pdf/volume2/diff_fund_2(2005)60.pdf
[26] Wilkening M, Küchler W and Heitjans P 2006 *Phys. Rev. Lett.* **97** 065901
[27] Böhmer R 2000 *J. Mag. Reson.* **147** 78
[28] Stebbins J F, Xu Z and Vollath D 1995 *Solid State Ion.* **78** L1
[29] Smaihi M, Petit D, Korb J P and Boilot J P 1991 *J. Solid State Chem.* **94** 260
[30] Smaihi M, Petit D, Gourbilleu F, Chaput F and Boilot J P 1991 *Solid State Ion.* **48** 213
[31] de Jong B H W S, Ellerbroeck D and Spek A L 1994 *Acta Crystallogr.* B **50** 511
[32] Xu X X and Wen Z Y 2005 *J. Inorg. Mater.* **20** 21
[33] Whitacre J F and West W C 2004 *Solid State Ion.* **175** 251
[34] Mizuno F, Hayashi A, Tadanaga K, Minami T and Tatsumisago M 2004 *Solid State Ion.* **175** 699
[35] Roux N, Johnson C and Noda K 1992 *J. Nucl. Mater.* **191** 15
[36] van der Laan J G, Kawamura H, Roux N and Yamaki D 2000 *J. Nucl. Mater.* **283** 99
[37] Kato M, Yoshikawa K and Nakagawa K 2002 *J. Mater. Sci. Lett.* **21** 485
[38] Gauer C and Heschel W 2006 *J. Mater. Sci.* **41** 2405
[39] Freude D and Haase J 1993 Quadrupole effects in solid-state nuclear magnetic resonance *NMR—Basic Principles and Progress* vol 29, ed P Diehl, E Fluck, H Günther, R Kosfeld and J Seelig (Berlin: Springer)
[40] Fujara F, Wefing S and Spiess H W 1986 *J. Chem. Phys.* **84** 4579
[41] Fleischer G and Fujara F 1994 NMR as a generalised incoherent scattering experiment *NMR—Basic Principles and Progress* vol 30, ed P Diehl, E Fluck, H Günther, R Kosfeld and J Seelig (Berlin: Springer)
[42] Jeener J and Broekaert P 1967 *Phys. Rev.* **157** 232
[43] Körblein A, Heitjans P, Stöckmann H J, Fujara F, Ackermann H, Buttler W, Dörr K and Grupp H 1985 *J. Phys. F: Met. Phys.* **15** 561
[44] Kanert O and Mehring M 1971 Static quadrupole effeccts in disordered cubic solids *NMR—Basic Principles and Progress* vol 3, ed P Diehl, E Fluck and R Kosfeld (Berlin: Springer)
[45] Grüne M, Müller-Warmuth W, Zum Hebel P and Krebs B 1993 *Solid State Ion.* **66** 165
[46] Wilkening M 2005 *PhD Thesis* University of Hannover
[47] Tranqui D, Shannon R D, Chen H Y, Iljima S and Baur W H 1979 *Acta Crystallogr.* B **35** 2479
[48] Hubbard P S 1970 *J. Phys. Chem.* **53** 985
[49] West A R 1967 *J. Appl. Electrochem.* **3** 327
[50] Hodge I M, Ingram M D and West A R 1976 *J. Am. Ceram. Soc.* **59** 360